EINDHOVEN
UNIVERSITY OF
TECHNOLOGY

Atomic layer deposition of high-k dielectric layers on Ge and III-V MOS channels

Citation for published version (APA):
Delabie, A., Alian, A., Bellenger, F., Brammertz, G., Brunco, D. P., Caymax, M., Conard, T., Franquet, A., Houssa, M., Sioncke, S., Elshocht, van, S., Hemmen, van, J. L., Keuning, W., Kessels, W. M. M., Afanasev, V. V., Stesmans, A., Heyns, M. M., & Meuris, M. (2008). Atomic layer deposition of high-k dielectric layers on Ge and III-V MOS channels. *ECS Transactions*, *16*(10), 671-685. https://doi.org/10.1149/1.2986824

DOI:
10.1149/1.2986824

Document status and date:
Published: 01/01/2008

Document Version:
Publisher's PDF, also known as Version of Record (includes final page, issue and volume numbers)

Please check the document version of this publication:

• A submitted manuscript is the version of the article upon submission and before peer-review. There can be important differences between the submitted version and the official published version of record. People interested in the research are advised to contact the author for the final version of the publication, or visit the DOI to the publisher's website.
• The final author version and the galley proof are versions of the publication after peer review.
• The final published version features the final layout of the paper including the volume, issue and page numbers.

Link to publication

General rights
Copyright and moral rights for the publications made accessible in the public portal are retained by the authors and/or other copyright owners and it is a condition of accessing publications that users recognise and abide by the legal requirements associated with these rights.

• Users may download and print one copy of any publication from the public portal for the purpose of private study or research.
• You may not further distribute the material or use it for any profit-making activity or commercial gain
• You may freely distribute the URL identifying the publication in the public portal.

If the publication is distributed under the terms of Article 25fa of the Dutch Copyright Act, indicated by the "Taverne" license above, please follow below link for the End User Agreement:

www.tue.nl/taverne

Take down policy
If you believe that this document breaches copyright please contact us at:

openaccess@tue.nl

providing details and we will investigate your claim.

Download date: 05. Oct. 2023

ECS Transactions, 16 (10) 671-685 (2008)
10.1149/1.2986824 ©The Electrochemical Society

Atomic layer deposition of high-κ dielectric layers on Ge and III-V MOS channels

A. Delabie[a], A. Alian[a], F. Bellenger[a], G. Brammertz[a], D. P. Brunco[b], M. Caymax[a], T. Conard[a], A. Franquet[a], M. Houssa[a], S. Sioncke[a], S. Van Elshocht[a], J. L. van Hemmen[c], W. Keuning[c], W.M.M. Kessels[c], V. V. Afanas'ev[d], A. Stesmans[d], M. M. Heyns[a], M. Meuris[a]

[a] IMEC, Kapeldreef 75, B-3001 Leuven, Belgium
[b] Intel assignee at IMEC
[c] Eindhoven University of Technology, Eindhoven, The Netherlands
[d] Department of Physics, University of Leuven, Leuven, Belgium

Ge and III-V semiconductors are potential high performance channel materials for future CMOS devices. In this work, we have studied Atomic Layer Deposition (ALD) of high-κ dielectric layers on Ge and GaAs substrates. We focus at the effect of the oxidant (H_2O, O_3, O_2, O_2 plasma) during gate stack formation. GeO_2, obtained by Ge oxidation in O_2 or O_3, is a promising passivation layer. The germanium oxide thickness can be scaled down below 1 nm, but such thin layers contain Ge in oxidation states lower than 4+. Still, electrical results indicate that small amounts of Ge in oxidation states lower than 4+ are not detrimental for device performance. Partial intermixing was observed for high-κ dielectric and GeO_2 or $GaAsO_x$, suggesting possible correlations in the ALD growth mechanisms on Ge and GaAs substrates.

Introduction

Hafnium-based oxide, deposited by Atomic Layer Deposition (ALD), has recently been implemented as the gate dielectric in 45-nm CMOS devices (1). To further increase transistor performance, high-κ gate dielectrics may be combined with Ge and III-V channel materials, which have higher intrinsic carrier mobilities as compared to Si. One of the issues when integrating high-κ dielectrics with Ge or III-V channels is obtaining a low defect density at the Ge or III-V interface. Initial devices fabricated on Ge substrates with high-κ dielectric layers aimed at preventing an interfacial oxide layer between the Ge channel and the high-κ dielectric in order to minimize the equivalent oxide thickness (EOT) of the gate stack. However, the interface state densities of such devices were much too high for device applications (2). In subsequent work, passivating interfacial layers between the Ge channel and the high-κ dielectric were developed, for example a thin (~0.6 nm) epitaxial Si passivation layer (3,4), germanium oxynitride (5), and S-passivation (6, 7).

Passivation of Ge using germanium oxide has been discarded for some time because the limited stability of GeO_2 and its solubility in water complicate device fabrication. Yet, recent reports show good passivation using germanium oxide both on n- and p-type Ge. Applying GeO_2 prepared by electron-cyclotron-resonance plasma irradiation resulted in an interface trap density (D_{it}) of $\sim 6 \times 10^{10}$ $cm^{-2}eV^{-1}$ at the midgap, measured by the ac

Downloaded 09 Feb 2009 to 131.155.151.59. Redistribution subject to ECS license or copyright; see http://www.ecsdl.org/terms_use.jsp

conductance method (8). Thermal oxidation and photo-oxidation of Ge were also investigated (8, 9, 10, 11). Thermally grown GeO_2 was shown to be an effective passivation layer in combination with HfO_2 and Al_2O_3 deposited by ALD (12, 13, 14). In the oxide, Ge was present in the 4+ oxidation state, and densities of interface states as low as mid 10^{11} $cm^{-2}eV^{-1}$ were achieved. Ge/GeO_x/CeO_2 and Ge/GeO_x/CeO_2/HfO_2 gate stacks grown by molecular beam deposition exhibited similar interface state densities even though the GeO_x layer contained Ge in low (2+ and 3+) oxidation states (15). On InGaAs, promising electrical properties in terms of leakage current and interface state density were claimed for Al_2O_3 layers deposited by ALD (16, 17). The reduction of Fermi-level pinning of the gate insulator/channel interface was ascribed to the removal of arsenic oxides during the ALD process.

ALD is often used to deposit high-κ dielectrics on Ge and III-V materials as the electrical quality of the Ge or III-V interfaces can be controlled at the typically low deposition temperature (18). In this work, we investigate structures formed by ALD of Al_2O_3 and HfO_2 on Ge and GaAs substrates. We focus on the role of the oxidant (H_2O, O_3, O_2, O_2 plasma) during gate stack formation. We have characterized the oxide layer before and after ALD of the high-κ dielectric on Ge and GaAs substrates. The oxidation states, oxide thickness, impurities, and possible intermixing with the high-κ dielectric are investigated. The aim of this work is to understand how to control the attained interfacial oxide layer during gate stack formation, and finally to identify electrically active defects limiting the ultimate electrical performance.

Experimental details

Ge(100) or Ge-on-Si substrates were cleaned in HF solution. The subsequent surface preparation, germanium oxidation, and high-κ deposition were performed in a Polygon® cluster (19) without air exposure between these process steps. Germanium oxidations in O_2 were explored in a Polygon 8200 cluster, equipped with an EPSILON™ reactor for thermal treatments and a PULSAR® 2000 reactor for ALD. The samples were first annealed in H_2 at 650°C for 10 minutes to desorb O or C that can be present after HF clean (20). Oxidations were subsequently performed in the same reactor in O_2 at 700 Torr at temperatures between 300 and 450°C. HfO_2 and Al_2O_3 layers were deposited on the GeO_2 layers at 300°C in the ALD reactor from $HfCl_4$ or $Al(CH_3)_3$ (trimethylaluminium or TMA) with H_2O. Germanium oxidations in O_3 were performed in a PULSAR® 3000 reactor, with subsequent H_2O or O_3 based ALD of HfO_2 or Al_2O_3 in the same reactor. For this end, 15% O_3 was generated in an O_2/N_2 mixture and 0.5 slm of this flow was further diluted with 2 slm N_2 in the ALD reactor. The pressure in the ALD reactor was ~1 Torr.

GaAs substrates were cleaned before ALD in HCl or $(NH_4)_2S$ solutions. Immediately after the clean, the wafers were blown dry with a N_2 gun. Depositions were also performed on the native oxide on GaAs. Thermal ALD of HfO_2 and Al_2O_3 were performed using $HfCl_4$ or TMA with H_2O in an ASM PULSAR® 2000 reactor at 300°C (19). Plasma Enhanced ALD (PEALD) of Al_2O_3 using TMA and O_2 plasma was performed in an Oxford Instruments FlexAl® reactor (21) at 300°C.

Angle Resolved X-ray Photoelectron Spectroscopy (AR-XPS) was carried out in a Theta300 system (Thermo Instruments) in parallel angle resolved mode using monochromatized Al K_a radiation. Oxide thicknesses were also verified with

Downloaded 09 Feb 2009 to 131.155.151.59. Redistribution subject to ECS license or copyright; see http://www.ecsdl.org/terms_use.jsp

spectroscopic ellipsometry (SE). The areal density of Hf (Hf/nm^2) on GeO_2 was measured by Rutherford Backscattering (RBS) in a RBS400 endstation with a 1 MeV He^+ beam. The areal density of Al (Al/nm^2) on GaAs was measured by Total X-ray Reflection Fluorescence (TXRF) in a TEI-Atomika 8300W system. Time of Flight Secondary Ion Mass Spectroscopy (TOFSIMS) was used for depth profiling, using a dual ion beam set up with a 500eV Xe+ ion beam.

Electrical measurements were performed on MOS capacitors with Pt gates. 50 nm thick Pt dots of different sizes were deposited by thermal evaporation using a shadow mask. The electrical characteristics were measured with a Keithley K4200 semiconductor parameter analyzer and a HP4284 LCR meter. The EOT was estimated by fitting the capacitance-voltage (CV) curves using the Hauser routine, including quantum mechanical corrections (22).

Oxidation of Ge in O_2 and O_3

Ge substrates were oxidized in either O_2 or O_3. The oxidation was carried out at a relatively low temperature range (225 – 450°C) in order to avoid decomposition of GeO_2 and desorption of GeO. For the O_2 case, the pressure was set at 700 Torr of O_2 in order to achieve a sufficiently high oxidation rate. The oxidation of Ge by O_3 was preformed in the ALD reactor at a nominal O_3 partial pressure of 0.04 Torr (not taking into account decomposition by transport from the O_3 generator to the reactor and thermal decomposition, as described below).

The oxidation rate in O_3 and O_2 are compared in Figure 1. For O_2, the oxidation rate increases with temperature in the temperature range 300-450°C and follows the Deal-Grove model, as described previously (23). When comparing oxidation in O_3 and O_2 at 300°C, we observe that O_3 oxidation proceeds slightly faster than O_2 oxidation even though the partial pressure of O_3 was much lower. O_3 is more reactive than O_2 because O_3 dissociates at the Ge surface to produce atomic oxygen thus enhancing oxidation (24):

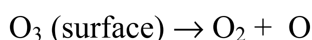

$$O_3 \text{ (surface)} \rightarrow O_2 + O$$

Still, the oxidation rate in O_3 is relatively slow in the studied temperature range (225 - 370°C), likely because of the low pressure of O_3.

O_3 oxidation shows a maximum rate at ~300°C: the oxidation rate increases when increasing the temperature from 225 to 300°C, and then again decreases slightly when further increasing the temperature to 370°C (Figure 1). The oxidation rate of Ge by atomic oxygen increases with temperature. The reduced oxidation rate at 370°C cannot be associated with GeO desorption as GeO is known to desorb only at temperatures higher than 420°C (25). Moreover, the decrease in oxidation rate was also observed for oxidation of Si in O_3 in the same conditions, and SiO desorption occurs at an even higher temperature range. Another possible explanation for the lower oxidation rate at 370°C is a lower concentration of O_3. Indeed, the lifetime of O_3 decreases with temperature (24). Before O_3 arrives at the Ge or Si surface, O_3 can thermally decompose by collisions with other gas molecules (M):

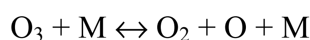

$$O_3 + M \leftrightarrow O_2 + O + M$$

Downloaded 09 Feb 2009 to 131.155.151.59. Redistribution subject to ECS license or copyright; see http://www.ecsdl.org/terms_use.jsp

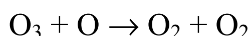

$$O_3 + O \rightarrow O_2 + O_2$$

Also, O_3 can be lost at the walls of the reactor

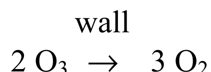

$$2\,O_3 \xrightarrow{\text{wall}} 3\,O_2$$

Which destruction reactions of O_3 are predominant will to a large extent depend on the geometry of the reactor. As the oxidations were performed in an ALD reactor where the distance between the wafer and the top wall is only a few mm, we expect a large contribution of wall destruction of O_3 especially at higher temperature. Indeed, the SiO_2 layer obtained at 370°C showed a decrease in thickness in the direction of the gas flow. The oxide layers grown at 225 and 300°C demonstrated good thickness uniformity (1 – 4% standard deviation) both for Si and Ge.

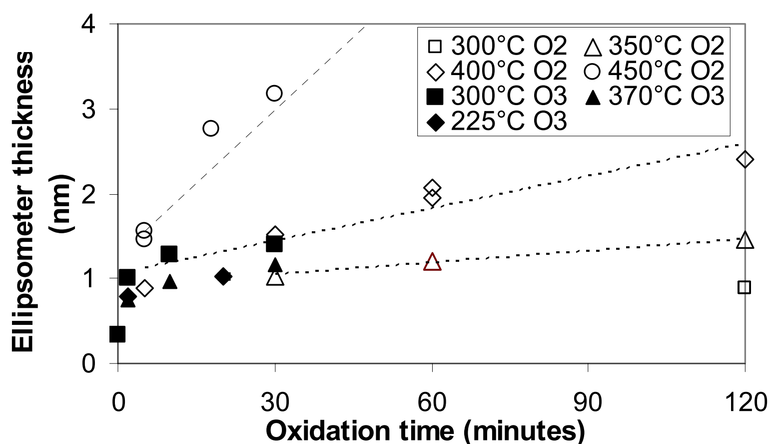

Figure 1. Germanium oxide thickness as a function of oxidation time for oxidation of Ge substrates in O_3 and O_2 at several temperatures, determined by ellipsometry. Trend lines are indicated as a guide to the eye.

The oxidation states of Ge in the germanium oxide layers grown in O_2 or O_3 were investigated by means of XPS. Note that XPS measurements were performed ex-situ, but air exposure between germanium oxidation and loading the samples in the XPS tool was limited to less than ~15 minutes. In order to determine the oxidation states of Ge in the oxide, the Ge3d spectrum was fitted using binding energy shifts of 0.8, 1.8, 2.6, and 3.4 eV for Ge3d in the 1+, 2+, 3+, and 4+ oxidation states (26). As described in reference (15), precise determination of the fraction of Ge in different oxidation states is complicated by the uncertainty in the XPS fitting and interpretation. The XPS fits should therefore be used as a qualitative guide to the key oxidation states, not for quantitative estimation of the ratios of Ge oxidation states. The fraction of Ge^{4+} (at% Ge^{4+} / (at% Ge^{1+} + at% Ge^{2+} + at% Ge^{3+} + at% Ge^{4+}) is plotted as a function of the GeO_x thickness in Figure 2, while a summary of all oxidation states is shown in TABLE 1.

The fraction of Ge^{4+} in the germanium oxide layers grown in both O_3 and O_2 depends clearly on the thickness of the germanium oxide layer, and less on the oxidation conditions (temperature, O_2, O_3, etc.) (Figure 2). For all germanium oxide layers thicker than ~1 nm, obtained either in O_2 or O_3, Ge^{4+} is the predominant oxidation state. The

Downloaded 09 Feb 2009 to 131.155.151.59. Redistribution subject to ECS license or copyright; see http://www.ecsdl.org/terms_use.jsp

highest fraction of Ge^{4+} was observed for the thickest germanium oxide layers grown in O_2 at 450°C. The 1 nm germanium oxide grown at 300°C in O_3 also contained Ge mainly in the form of Ge^{4+}, only a small fraction of Ge^{2+} was present.

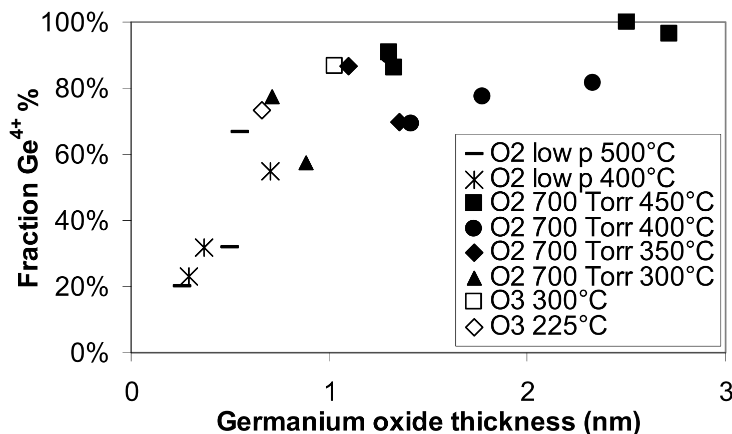

Figure 2. Fraction of Ge^{4+} (at% Ge^{4+}/(at% Ge^{1+} + at% Ge^{2+} + at% Ge^{3+} + at% Ge^{4+}) as a function of the germanium oxide thickness (XPS) for different oxidation conditions (see TABLE 1).

TABLE 1. Summary of the Ge oxidation states in GeO_x layers obtained by thermal oxidation in O_2 or O_3, as determined by XPS.

Oxidation conditions	Ge^{1+} (at%)	Ge^{2+} (at%)	Ge^{3+} (at%)	Ge^{4+} (at%)	GeO_x thickness (nm)
O_2 700 Torr 300°C 120 min	22%	0%	20%	57%	0.88
O_2 700 Torr 300°C 120 min	15%	1%	7%	77%	0.71
O_2 700 Torr 350°C 60 min	7%	7%	0%	86%	1.10
O_2 700 Torr 350°C 120 min	12%	3%	15%	70%	1.35
O_2 700 Torr 400°C 30 min	12%	3%	16%	69%	1.41
O_2 700 Torr 400°C 60 min	10%	0%	12%	77%	1.77
O_2 700 Torr 400°C 60 min	5%	3%	3%	90%	1.30
O_2 700 Torr 400°C 120 min	7%	0%	11%	82%	2.33
O_2 700 Torr 450°C 5 min	3%	6%	0%	91%	1.30
O_2 700 Torr 450°C 18 min	0%	0%	0%	100%	2.50
O_2 700 Torr 450°C 5 min	0%	8%	6%	86%	1.33
O_2 700 Torr 450°C 30 min	0%	0%	4%	96%	2.72
O_2 700 Torr 450°C 60 min	0%	0%	8%	92%	4.20
O_2 0.06 Torr 400°C 5 min	0%	25%	43%	32%	0.37
O_2 12 Torr 400°C 5 min	8%	6%	32%	55%	0.70
O_2 0.06 Torr 500°C 5 min	0%	20%	48%	32%	0.50
O_2 12 Torr 500°C 5 min	0%	12%	21%	67%	0.55
O_3 225°C 30 min	8%	12%	6%	73%	0.66
O_3 300°C 30 min	0%	13%	0%	87%	1.03

Layers thinner than ~1 nm contain a higher fraction of lower oxidation states. Which oxidation states are present depends on the oxidation conditions. Thin layers grown in 700 Torr O_2 at 300°C contain, next to Ge^{4+}, about 10-20 % of Ge in the 1+ and 3+ oxidation states, while almost no Ge^{2+} is observed. On the other hand, thin germanium oxide layers grown at lower O_2 pressure (0.06 – 12 Torr) and higher temperature (400-500°C) contain Ge^{2+} and Ge^{3+} and almost no Ge^{1+}. The presence of Ge^{2+} in the thin

Downloaded 09 Feb 2009 to 131.155.151.59. Redistribution subject to ECS license or copyright; see http://www.ecsdl.org/terms_use.jsp

oxides grown at higher temperature is surprising considering that desorption of GeO can occur at temperatures higher than 420°C (25). On the other hand, no Ge^{2+} is found in the samples grown at lower temperature. This may be related to the much longer oxidation time due to the low oxidation rate of O_2. The 0.7 nm germanium oxide layer grown in O_3 at 225°C contains predominantly Ge^{4+}, while small fractions of Ge^{1+}, Ge^{2+} as well as Ge^{3+} are observed.

ALD of HfO_2 and Al_2O_3 on GeO_2 and Ge substrates

O_3 and H_2O based ALD of both HfO_2 and Al_2O_3 was performed on thermally grown GeO_2 layers, and on HF cleaned Ge substrates for comparison. Air exposure of GeO_2 was avoided by performing the oxidation and ALD in clustered reactors. The ALD was performed at relatively low temperature (300°C or lower) to avoid GeO desorption. Still, the ALD has an impact on the thickness of the GeO_2 layer, the abruptness of the Ge/GeO_2/high-κ interfaces, and the predominant oxidation states of Ge.

Effect of ALD precursors on the germanium oxide interfacial layer thickness

In order to investigate the effect of the ALD precursors and process conditions on the thickness of the germanium oxide interfacial layer, we considered ALD on 1 nm GeO_2 layers (obtained by 20 minutes O_3 oxidation at 300°C) and on HF cleaned Ge substrates (0.2 – 0.3 nm GeO_x remains present on HF cleaned Ge substrates). The GeO_2 thickness was measured by means of XPS, and the results are summarized in Figure 3.

No further oxidation of Ge occurs during H_2O based ALD, both for $HfCl_4$/H_2O and TMA/H_2O ALD, as reported previously (27). On thermally grown GeO_2, the GeO_2 thickness remains ~ 1 nm after the H_2O based ALD. Also the thin GeO_x layer present after HF clean does not grow further during H_2O based ALD.

On the other hand, the Ge substrate oxidizes during O_3 based ALD. This is most noticeable for deposition on HF cleaned Ge. A 0.7 nm germanium oxide layer is formed when using the TMA/O_3 ALD. An even thicker germanium oxide layer, 1.7 nm, is formed during $HfCl_4$/O_3 ALD. First, the differences in germanium oxide thickness for the two processes can be related to differences in O_3 pulse times. In the $HfCl_4$/O_3 ALD, O_3 pulse times of at least 10 seconds are required to achieve a uniform HfO_2 layer (Figure 4a). On the other hand, O_3 pulse times of about 2 orders of magnitude shorter (< 500 ms) are used for TMA/O_3 process (Figure 4b), resulting in substantially less pronounced oxidation of the Ge substrate during the ALD. Second, the GeO_2 thickness after $HfCl_4$/O_3 ALD is even larger than for oxidation of Ge in O_3 at the same temperature, indicating a catalytic effect of Hf species at the Ge surface on the oxidation.

On 1 nm GeO_2, we observe a similar difference between the TMA/O_3 and $HfCl_4$/O_3 ALD. The GeO_2 thickness is not affected by the TMA/O_3 process, while for the $HfCl_4$/O_3 ALD the GeO_2 thickness increases to 1.7 nm, the same value as for deposition on HF cleaned Ge. Thus, the GeO_2 thickness is independent on the starting surface for $HfCl_4$/O_3 ALD due to the excessive re-growth of GeO_2 during ALD. The re-growth during $HfCl_4$/O_3 ALD can be decreased by decreasing the ALD temperature from 300 to 225°C, where only 1.2 nm GeO_2 is observed. Decreasing the deposition temperature for TMA/O_3 from 300 to 225°C does not result in a significant thickness decrease.

Downloaded 09 Feb 2009 to 131.155.151.59. Redistribution subject to ECS license or copyright; see http://www.ecsdl.org/terms_use.jsp

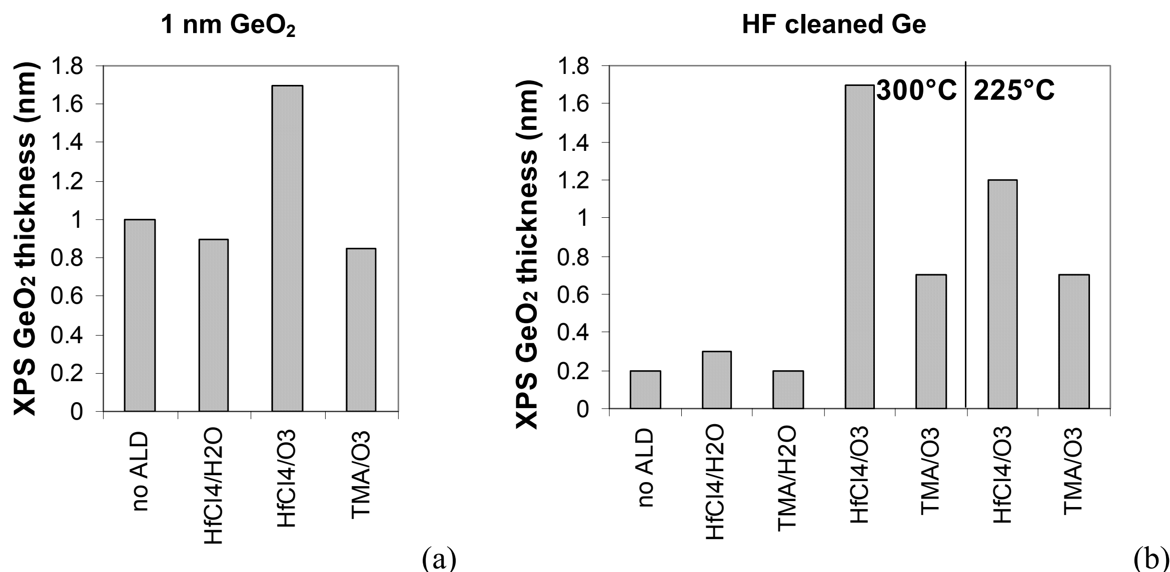

Figure 3. GeO_2 thickness determined by XPS after ALD of 2 nm HfO_2 or Al_2O_3 (a) on 1 nm GeO_2 (20 minutes O_3 at 300°C) (b) on HF cleaned Ge.

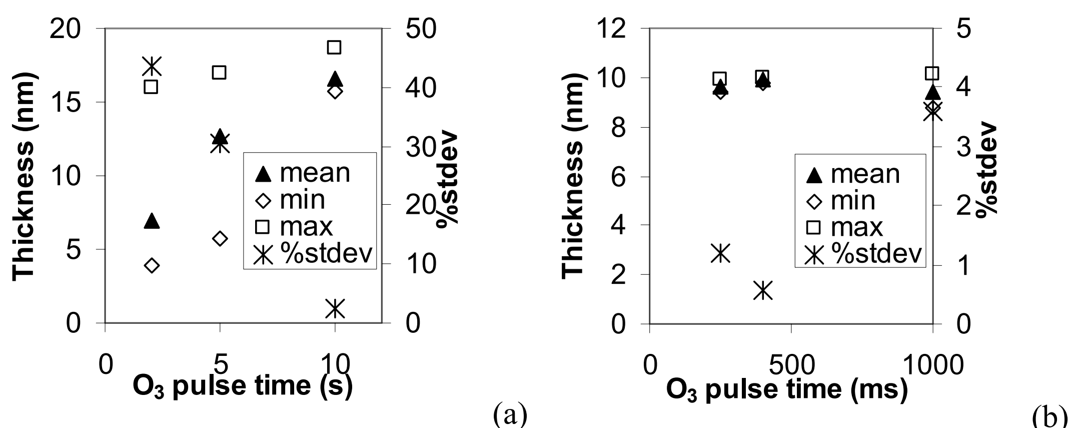

Figure 4. Effect of O_3 pulse time on thickness and uniformity (49 points on 300 mm Si wafer); (a) 100 cycles $HfCl_4/O_3$ ALD at 300°C; (b) 100 cycles TMA/O_3 ALD at 300°C.

<u>Effect of ALD precursors on the abruptness of Ge/GeO_x/high-κ interfaces</u>

The quality of the interfaces between Ge/GeO_x/high-κ and the extent of intermixing of the GeO_2 and high-κ layer also depend on the ALD process parameters, as demonstrated by TOFSIMS depth profiling. We report Ge^+ profiles for different ALD layers in Figure 5, similar trends were observed for the GeO^+ profiles.

For HfO_2 and Al_2O_3 ALD on 1 nm GeO_2, we observe partial intermixing of GeO_2 with the high-κ dielectric, both for GeO_2 grown in O_2 (12) and in O_3 (Figure 5a, Figure 5b). Still, the amount of GeO_x in the high-κ layers is small (note the exponential scale in the TOFSIMS Ge^+ profiles). For example, for Al_2O_3, the intensity of the Ge^+ signal is diminished by one order of magnitude at a distance of 1 nm from the GeO_2 interface, indicating about 3 at% of Ge. This may explain why this small degree of intermixing was not observed previously by means of AR-XPS (12), while TOFSIMS is sensitive enough to detect it. Still, such small concentrations of Ge in the high-κ layer can affect the

Downloaded 09 Feb 2009 to 131.155.151.59. Redistribution subject to ECS license or copyright; see http://www.ecsdl.org/terms_use.jsp

electrical properties. Note that TOFSIMS cannot determine the oxidation state of Ge in the high-κ layer, but most likely it is present in an oxidized state and not as Ge^0, as TOFSIMS demonstrated previously that $HfCl_4/H_2O$ ALD on HF cleaned Ge substrates results in an abrupt Ge/HfO_2 transition (27). First principles calculations demonstrated that the formation of Ge–O bonds or Hf–O–Ge bonds at or near the interface does not introduce interface states to the Ge energy band-gap (28, 29). On the other hand, it was suggested that such bonds could be responsible for hysteresis often observed in CV curves (23).

For Al_2O_3 ALD, the amount of intermixing is independent of the oxidant precursor (H_2O or O_3, Figure 5a). In contrast, for HfO_2 ALD the extent of intermixing depends on the oxidant: the layers intermix more with O_3 than H_2O based ALD (Figure 5b). For the O_3 based process, the intermixing decreases slightly when decreasing the ALD temperature from 300 to 225°C. The presence of GeO_x in the high-κ layer indicates that reactions other than the conventional ligand exchange reactions must contribute during ALD on GeO_2, as suggested previously for $HfCl_4/H_2O$ ALD on 0.3 nm GeO_x by considering the first reaction cycle (27).

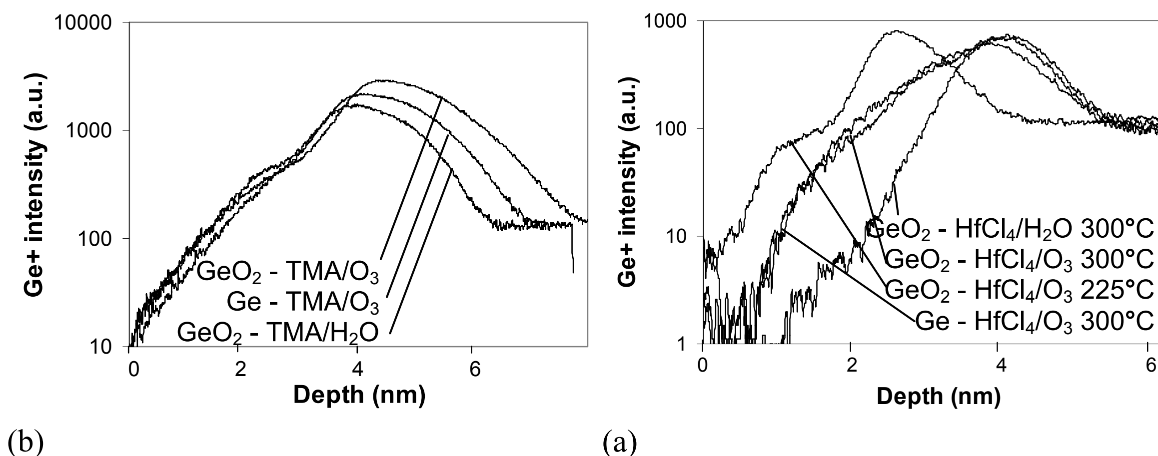

(b) (a)

Figure 5. TOFSIMS depth profiles of ~4 nm high-κ layers on Ge substrates: (a) TMA/H_2O and TMA/O_3 on GeO_2 (20 min O_3 at 300°C) and on HF cleaned Ge; (b) $HfCl_4/H_2O$ and $HfCl_4/O_3$ ALD on GeO_2 (20 min O_3 at 300°C) and on HF cleaned Ge.

Effect of ALD precursors on the oxidation states of Ge

Not only the thickness but also the oxidation states of Ge in the interfacial germanium oxide layer can be affected by ALD of the high-κ dielectric. We have analyzed this effect for Al_2O_3 ALD on GeO_2 by investigating the XPS Ge3d spectra. Unfortunately, a similar analysis cannot be performed for HfO_2 ALD as the Ge3d peak is located at a binding energy very close to the O2s peak from HfO_2 (32.5 eV). The quantitative determination of the oxidation states of Ge is complicated by the presence of the high-κ layer (partial intermixing as described above and potential charge effects). Therefore, instead of deconvolution of the Ge3d signal, we compare the apparent binding energy shift of the germanium oxide 3d peak (Figure 6). The smaller the binding energy shift, the higher the fraction of low oxidation states in the oxide; the larger the binding energy shift, the higher the fraction of high oxidation states in the oxide.

Downloaded 09 Feb 2009 to 131.155.151.59. Redistribution subject to ECS license or copyright; see http://www.ecsdl.org/terms_use.jsp

For Al_2O_3 ALD on GeO_2 layers with thicknesses larger than 1 nm, the main oxidation state of Ge remains Ge^{4+}, indicated by a binding energy shift of the oxidized Ge3d peak of ~3 eV (Figure 6). Thus, contributions of Ge in oxidation states lower than 4+ are small. The binding energy shift decreases when decreasing the thickness of germanium oxide below 1 nm, suggesting the occurrence of Ge in oxidation states of 4+ and lower. This observation is similar to that made for the GeO_2 layers without high-κ dielectrics on top (Figure 2). Thus, when scaling down the thickness of germanium oxide for EOT reduction, lower oxidation states may occur in germanium oxide.

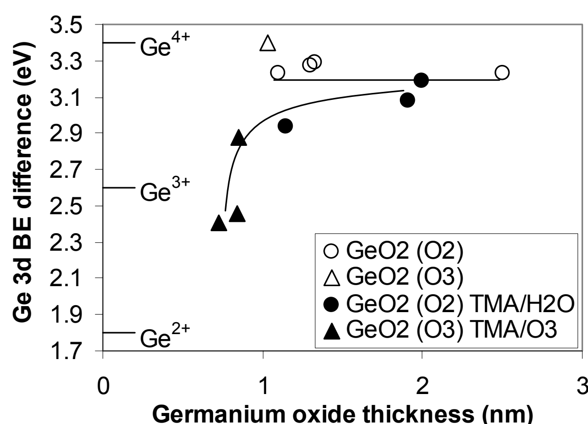

Figure 6. XPS binding energy shift of the Ge3d oxide peak (relative to the substrate peak) as a function of the germanium oxide thickness for GeO_2 layers and for GeO_2 covered with 2 nm of Al_2O_3. Trend lines are indicates as a guide to the eye. Binding energy shifts of for Ge3d in the 2+, 3+, and 4+ oxidation states (26) are indicated as a guides to oxidation states that can be present.

Electrical characteristics of devices with GeO_2 interfacial layers

Capacitance-Voltage characteristics

Capacitance-Voltage characteristics for Pt gated capacitors with 4-nm thick high-κ dielectrics (H_2O or O_3 based ALD) are compared in Figure 7. The CV characteristics of the capacitors shown here behave nicely. Frequency dispersion in accumulation at higher frequencies is observed due to series resistance as undoped Ge-on-Si wafers were used.

The measured EOT of the capacitors is summarized in Table 2. The determined EOT values are in excellent agreement with EOT estimations based on the thickness of the high-κ (4 nm) and GeO_2 (XPS), assuming a κ-value of 6 for GeO_2 (30), 20 for HfO_2 (31) and 9 for Al_2O_3 (32).

The lowest EOT, 1.5 nm, was obtained for 4 nm $HfCl_4/H_2O$ ALD deposited on 1 nm GeO_2. As shown above, the $HfCl_4/H_2O$ ALD has the advantage of no additional oxidation of Ge during ALD. A higher EOT, 2.0 nm, is obtained for $HfCl_4/O_3$ ALD, due to the presence of a thicker GeO_2 layer (1.7 nm). XPS indicated that decreasing the ALD temperature for the $HfCl_4/O_3$ process results in a thinner GeO_2 layer. However, devices with $HfCl_4/O_3$ deposited at 225°C demonstrated a high leakage current, making these films unsuitable for gate dielectric applications. TOFSIMS indicated that the Cl-content was more than 1 order of magnitude higher for O_3 or H_2O based ALD at 300°C.

Downloaded 09 Feb 2009 to 131.155.151.59. Redistribution subject to ECS license or copyright; see http://www.ecsdl.org/terms_use.jsp

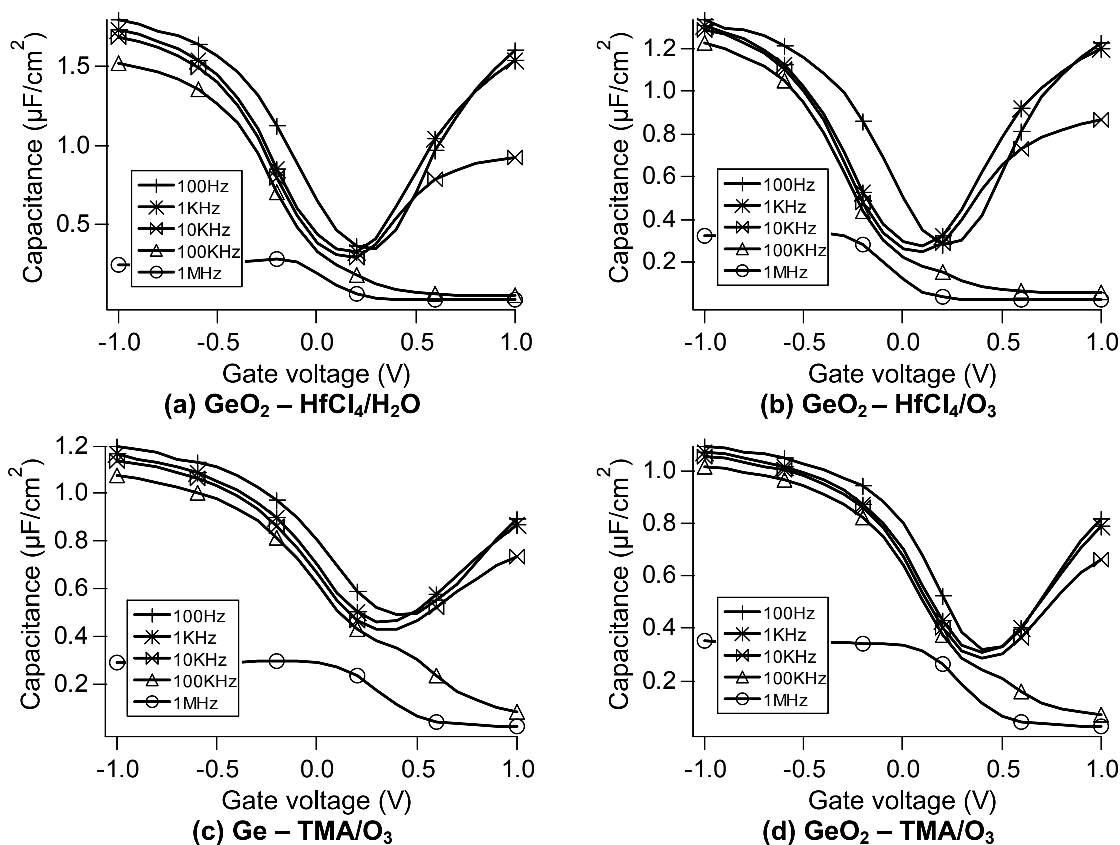

Figure 7. Capacitance-Voltage characteristics as a function of frequency (a) 4 nm HfO_2 ($HfCl_4/H_2O$) on 1 nm GeO_2 (20 min O_3 at 300°C); (b) 4 nm HfO_2 ($HfCl_4/O_3$) on 1 nm GeO_2 (20 min O_3 at 300°C); (c) 4 nm Al_2O_3 (TMA/O_3) on HF cleaned Ge; (d) 4 nm Al_2O_3 (TMA/O_3) on 1 nm GeO_2 (20 min O_3 at 300°C).

TABLE 2. Summary of EOT for capacitors with HfO_2 and Al_2O_3 dielectrics.

Starting surface	ALD	Temperature (°C)	Estimated EOT (nm)	Measured EOT (nm)
GeO_2 20 min O_3	$HfCl_4/O_3$	300	1.9	2.0
GeO_2 20 min O_3	$HfCl_4/H_2O$	300	1.4	1.5
HF cleaned Ge	TMA/O_3	300	2.2	2.4
GeO_2 20 sec O_3	TMA/O_3	300	2.3	2.4
GeO_2 20 min O_3	TMA/O_3	300	2.3	2.6

The TMA/O_3 process demonstrates the feasibility of obtaining a thin germanium oxide interfacial layer while keeping good CV characteristics. The EOT slightly decreases when the Ge oxidation time before ALD is reduced, due to a thinner germanium oxide layer (XPS). The CV characteristics are well behaved even for TMA/O_3 ALD directly on HF cleaned Ge (and starting the ALD with a TMA pulse) (Figure 7c). In this case, the interfacial oxide layer is only 0.7 nm, with Ge in oxidation states 4+ and lower. The CV characteristics are much better than those observed previously for H_2O based ALD on HF cleaned Ge, where large frequency dispersion and even flat CV characteristics were reported (2). As compared to the capacitors with ALD on 1 nm GeO_2 (Figure 7a, b, d), the CV curves are slightly more stretched out. Still, it is possible to achieve reasonable passivation with a thin germanium oxide interfacial layer where Ge oxidation states lower that 4+ are present.

Downloaded 09 Feb 2009 to 131.155.151.59. Redistribution subject to ECS license or copyright; see http://www.ecsdl.org/terms_use.jsp

Interface state densities of 1 – 3 10^{12} $cm^{-2}eV^{-1}$ were obtained for all devices shown in Figure 7 even without post deposition treatments, using the low-frequency or quasistatic method (33). Further electrical characterization is necessary in order to investigate the relation between interface state density and the Ge oxidation states, germanium oxide thickness or intermixing. Whether or not scaling down the thickness of GeO_2 underneath HfO_2 is feasible will be the subject of further investigation. Theoretical calculations indicate that the formation of a Ge–Hf bonds at the interface, likely present if Hf is located in the sub-oxide interfacial layer (GeO_x with $x < 2$), results in the formation of a defect level in the upper part of the Ge energy band-gap, degrading the electrical properties of metal-oxide-semiconductor devices (28).

$HfCl_4/H_2O$ ALD on 1 nm GeO_2 (Ge substrates) results in a similar leakage current as on 1 nm SiO_2 (Si substrates), as shown in Figure 8 that compares the leakage current – EOT behavior of the Ge devices with that of similar devices on Si substrates. The $HfCl_4/O_3$ ALD on Ge gives a higher EOT due to the thicker GeO_2 layer. Still, the leakage current for $HfCl_4/O_3$ and $HfCl_4/H_2O$ ALD is similar. Under gate injection, transport through the high-κ layer limits the current, and is expected to depend mainly on the physical thickness of the high-κ layer. The Al_2O_3 stacks also give a comparable leakage current at an even higher EOT due to the lower κ-value of Al_2O_3.

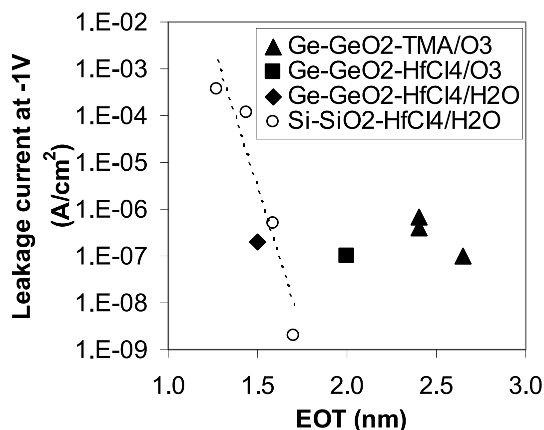

Figure 8. Leakage current as a function of EOT for Pt gated capacitors with 4 nm high-κ dielectrics on Ge substrates, and 2-5 nm of HfO_2 ALD on Si substrates ($HfCl_4/H_2O$ on 1 nm SiO_2).

The hysteresis in the CV characteristics is frequency dependent and varies from 70 mV to 250 mV for HfO_2 layers with and without pre-oxidation, as well as the Al_2O_3 layer without pre-oxidation. For the Al_2O_3 layer with O_3 pre-oxidation, the observed hysteresis varies less, from 70 mV to 100 mV. The hysteresis values are significantly lower than those reported previously for transistors with $Ge/GeO_2/HfO_2/TiN$ gate stacks, where process steps at higher temperatures were included (12).

Effect of ALD precursors on the band gap of GeO_2

Internal photoemission indicates that the oxidant used in the HfO_2 ALD affects the band gap of the GeO_2 layer. For $HfCl_4/O_3$ on GeO_2, the band gap measured for GeO_2 is close to the value reported for stoichiometric GeO_2 (5.5 eV). This was also demonstrated

Downloaded 09 Feb 2009 to 131.155.151.59. Redistribution subject to ECS license or copyright; see http://www.ecsdl.org/terms_use.jsp

previously for $HfCl_4/O_3$ at 375°C on Ge substrates (34) and was confirmed by our measurements for $HfCl_4/O_3$ at 300°C on GeO_2. On the other hand, the band gap of GeO_2 layer is reduced to 4.3 eV when HfO_2 is deposited on GeO_2 by means of H_2O based ALD (35), even for GeO_2 layers with a thickness of more than 2 nm. It was suggested that hydroxyl groups are incorporated in the GeO_2 layer during H_2O based ALD, and that the incorporation of OH in GeO_2 lowers the value of the band gap. Thus, whereas the H_2O based process has the advantage of no additional Ge oxidation during ALD, the O_3 based process has the advantage of preserving the value of the GeO_2 band gap.

ALD on GaAs substrates

The oxidant precursor also plays an important role in the formation of the interfacial layer on GaAs substrates. For the thermal process, XPS indicates no interfacial layer on GaAs for both HfO_2 and Al_2O_3 ALD (Figure 9 for Al_2O_3 ALD and reference 36 for HfO_2 ALD). The As3d oxide peak at binding energy of 43 – 46 eV decreases as a function of the Al_2O_3 thickness, and for Al_2O_3 layers of ~2 nm (60-70 Al/nm^2), no As_2O_5 or As_2O_3 were detected. So, the AsO_x-GaO_y layers that were present before ALD are removed during H_2O based ALD at 300°C, at least for the $HfCl_4/H_2O$ and TMA/H_2O ALD. Thinning of the initial oxide has also been reported previously for Al_2O_3 ALD (TMA/H_2O at 300°C) on GaAs and InGaAs (16, 17). On the other hand, the interfacial oxide thickness increased during PEALD using TMA and O_2 plasma (Figure 9). The XPS As3d and Ga3d spectra indicate that As_2O_3, As_2O_5, as well as Ga_2O_3 are present.

As and Ga partly intermix with the Al_2O_3 layers (Figure 10), similar as for ALD on GeO_2 substrates. Both the H_2O and O_2 plasma based Al_2O_3 ALD show a similar extent of intermixing. On the other hand, the $HfCl_4/H_2O$ ALD of HfO_2 on GaAs shows more abrupt interfaces, again in correspondence with ALD on GeO_2 (see above). These trends are observed for deposition on both native oxide and HCl cleaned GaAs. Although the reaction mechanisms accounting for incorporation of GeO_2, GaO_x and/or AsO_x are unclear, these results suggest that there are correlations in the reaction mechanisms on Ge and GaAs substrates.

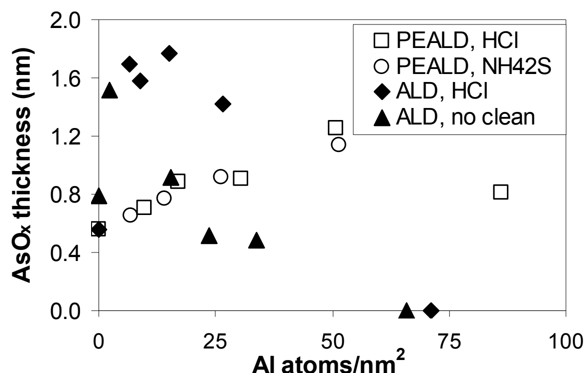

Figure 9. XPS AsO_x thickness as a function of Al-content for thermal and PEALD Al_2O_3 on GaAs with different surface preparations.

Downloaded 09 Feb 2009 to 131.155.151.59. Redistribution subject to ECS license or copyright; see http://www.ecsdl.org/terms_use.jsp

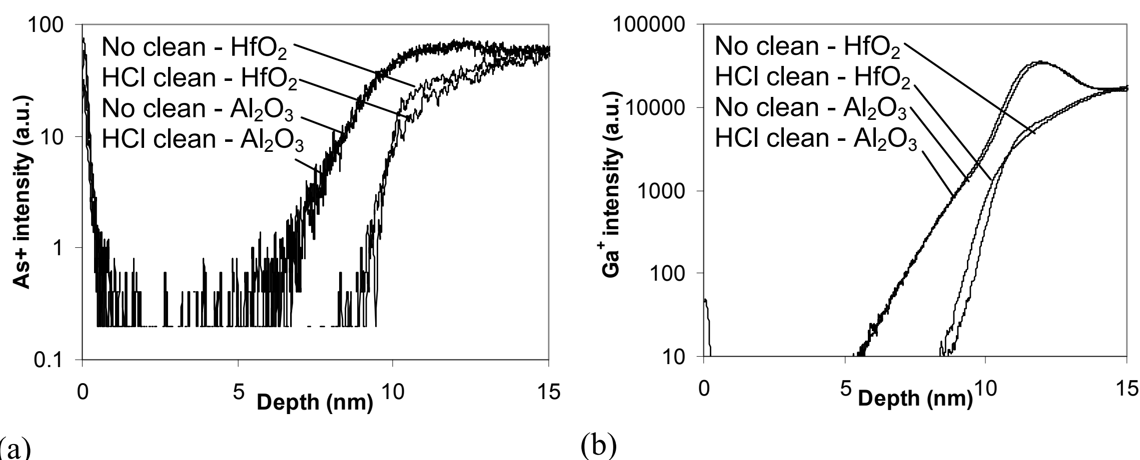

(a) (b)

Figure 10. TOFSIMS depth profiles for 10 nm HfO_2 and Al_2O_3 layers on GaAs without and with HCl clean. (a) As^+ intensity; (b) Ga^+ intensity.

Preliminary device measurements on GaAs/high-κ/Pt capacitors indicate that the oxide interfacial layer has an impact on the device characteristics: for the thermal ALD process, less frequency dispersion, less hysteresis and higher capacitance are observed, probably linked to the lower content of As_2O_3, As_2O_5 and Ga_2O_3 (37). Nevertheless, all interfaces (using both ALD and PEALD) are still Fermi level pinned, as discussed in (38) for Al_2O_3 deposited by thermal ALD, and in (37) for both thermal and plasma enhanced ALD. Together with the investigation of the ALD precursors, the effect of surface preparation before the ALD and post-deposition treatments should be further investigated.

Conclusions

The ALD precursors play an important role in the characteristics of both Ge and III-V MOS devices. Passivation of interface defects using thermally grown GeO_2 is a promising approach. We demonstrated that the thickness, oxidation states of Ge, and the amount of intermixing of germanium oxide with the high-κ dielectric depend on the ALD precursors and process conditions.

H_2O based ALD has the advantage of no additional Ge oxidation during ALD but internal photoemission indicates a low band gap of germanium oxide (4.3 eV), supposedly by hydroxyl incorporation during H_2O based ALD. On the other hand, $HfCl_4/O_3$ ALD at 300°C results in a rather thick (1.7 nm) GeO_2 interfacial layer. Oxidation of Ge can be minimized in ALD processes with shorter O_3 pulse times, for example TMA/O_3, and by reducing the ALD temperature. As such, the germanium oxide thickness was scaled down below 1 nm. However, such thin germanium oxide layers contain Ge in oxidation states lower than 4+. Still, electrical results indicate that small amounts of Ge in oxidation states lower than 4+ are not detrimental for device performance.

Partial intermixing was observed for high-κ ALD on both GeO_2 and $GaAsO_x$, suggesting possible correlations in the ALD growth mechanisms on Ge and GaAs substrates. Obtaining good device characteristics with ALD high-κ dielectrics on GaAs substrates remains nevertheless challenging. Together with the investigation of the

Downloaded 09 Feb 2009 to 131.155.151.59. Redistribution subject to ECS license or copyright; see http://www.ecsdl.org/terms_use.jsp

influence of the applied ALD precursors, the effect of surface preparation before the ALD and post-deposition treatments should be further investigated.

Acknowledgements

We acknowledge support by the European Commission's project FP7-ICT-DUALLOGIC no. 214579 "Dual-channel CMOS for (sub)-22 nm high performance logic".

References

1. M. Bohr, R. Chau, T. Ghani, and K. Mistry, *IEEC Spectrum*, **44**, 29 (2007).
2. M. Houssa, B. De Jaeger, A. Delabie, S. Van Elshocht, V. Afanasiev, J. Autran, A. Stesmans, M. Meuris, and M. Heyns, *J. Non-Crystal. Solids*, **351**, 1902 (2005).
3. P. Zimmerman, G. Nicholas, B. De Jaeger, B. Kaczer, L-Å Ragnarsson, D.P. Brunco, F. E. Leys, M. Caymax, G. Winderickx, K. Opsomer, M. Meuris, and M. M. Heyns, *IEDM Technical Digest*, Paper 26.1 (2006).
4. D. P. Brunco, B. De Jaeger, G. Eneman, J. Mitard, G. Hellings, A. Satta, V. Terzieva, L. Souriau, F. E. Leys, G. Pourtois, M. Houssa, G. Winderickx, E. Vrancken, S. Sioncke, K. Opsomer, G. Nicholas, M. Caymax, A. Stesmans, J. Van Steenbergen, P. W. Mertens, M. Meuris, and M. M. Heyns, *J. Electrochem. Soc.*, **155**, H552 (2008).
5. H. Kim, P. C. McIntyre, C. O. Chui, K. C. Saraswat, M.-H. Cho, *Appl. Phys. Lett.*, **85**, 2902 (2004).
6. M. M. Frank, S. J. Koester, M. Copel, J.A. Ott, V. K. Paruchuri, H. Shang, and R. Loesing, *Appl. Phys. Lett.*, **89**, 112905 (2006).
7. M. Caymax, S. Van Elshocht, M. Houssa, A. Delabie, T. Conard, F. Bellenger, R. Bonzom, F. Leys, D. Nelis, M. Meuris, M. Heyns, D. Brunco, P. Zimmerman, and A. Dimoulas, E-MRS IUMRS ICEM Spring Meeting, 29 May-2 June 2006; Nice, France.
8. Y. Fukuda, T. Ueno, S. Hirono, and S. Hashimoto, *Jap. J. Appl. Phys.*, **44**, 6981 (2005).
9. A. Molle, Md. N. K. Bhuiyan, G. Tallarida, and M. Fanciulli, *Appl. Phys. Lett.*, **89**, 083504 (2006).
10. Y. Wang, Y. Z. Hu, E. A. Irene, *J. Vac. Sci. Thechnol. A*, **12**, 1309 (1994).
11. V. Craciun, Ian W. Boyd, B. Hutton and D. Williams, *Appl. Phys. Lett.*, **75**, 1261 (1999).
12. A. Delabie, F. Bellenger, M. Houssa, T. Conard, S. Van Elshocht, M. Caymax, M. Heyns, M. Meuris, *Appl. Phys. Lett.*, **91**, 082904 (2007).
13. D. Kuzum, T. Krishnamohan, A. J. Pethe, A. K. Okyay, Y. Oshima, Y. Sun, J. P. McVittie, P. A. Pianetta, P. C. McIntyre, K. C. Saraswat, *IEEE Electron Dev. Lett.*, **29** 328-330 (2008).
14. T. Sugawara, Y. Oshima, R. Sreenivasan, and P. C. McIntyre, *Appl. Phys. Lett.*, **90**, 112912 (2007).
15. D. P. Brunco, A. Dimoulas, N. Boukos, M. Houssa, T. Conard, K. Martens, C. Zhao, F. Bellenger, M. Caymax, M. Meuris, and M. M. Heyns, *J. Appl. Phys.*, **102**, 024104 (2007).
16. P. D. Ye, G. D. Wilk, B. Yang, J. Kwo, S. N. G. Chu, S. Nakahara, H.-J. L. Gossmann, J. P. Mannaerts, M. Hong, K. K. Ng, and J. Bude, *Appl. Phys. Lett.*, **83**, 180 (2007).
17. M. L. Huang, Y. C. Chang, C. H. Chang, Y. J. Lee, P. Chang, J. Kwo, T. B. Wu and M. Hong, *Appl. Phys. Lett.*, **87**, 252104 (2005).

Downloaded 09 Feb 2009 to 131.155.151.59. Redistribution subject to ECS license or copyright; see http://www.ecsdl.org/terms_use.jsp

18. S. Van Elshocht, M. Caymax, T. Conard, S. De Gendt, I. Hoflijk, M. Houssa, F. Leys, R. Bonzom, B. De Jaeger, J. Van Steenbergen, W. Vandervorst, M. Heyns, and M. Meuris, *Thin Solid Films*, **508**, 1 (2006).
19. Polygon, EPSILON, ALCVD, and PULSAR are trademarks of ASM International, The Netherlands.
20. S. Rivillon, Y. J. Chabal, F. Amy, A. Kahn, *Appl. Phys. Lett.*, **87**, 253101 (2005).
21. J. L. van Hemmen, S. B. S. Heil, J. H. Klootwijk, F. Roozeboom, C. J. Hodson, M. C. M. van de Sanden, W. M. M. Kessels, *J. Electrochem Soc.*, **154**, G165 (2007).
22. J. R. Hauser et al., in *Characterization and Metrology for ULSI Technology*. p. 235 (1998).
23. F. Bellenger, M. Houssa, A. Delabie, V. Afanasiev, T. Conard, M. Caymax, M. Meuris, K. De Meyer, and M. M. Heyns, *J. Electrochem. Soc.*, **155**, G33 (2008).
24. T. Nishiguchi, Y. Sato, H. Nonaka, S. Ichimura, T. Noyori, Y. Morikawa, M. Kekura and Y. Nihei, *Jap. J. Appl. Phys.*, **44**, 118, 2005.
25. K. Prabhakaran, F. Maeda, Y. Watanabe, and T. Ogino, *Appl. Phys. Lett.*, **76**, 2244 (2000).
26. D. Schmeisser, R. D. Schnell, A. Bogen, F. J. Himpsel, D. Reiger, G. Landgren, and J. F. Morar, *Surf. Sci.*, **172**, 455 (1986).
27. A. Delabie, R. L. Puurunen, B. Brijs, M. Caymax, T. Conard, B. Onsia, O. Richard, W. Vandervorst, C. Zhao, M. M. Heyns, M. Meuris, M. Viitanan, H. Brongersma, M. de Ridder, L. Goncharova, E. Garfunkel, T. Gustafsson, and W. Tsai, *J. Appl. Phys.*, **97**, 064104 (2005).
28. M. Houssa, G. Pourtoi, M. Caymax, M. Meuris, M. M. Heyns, *Surf. Sci.*, **602**, L25 (2008).
29. M. Caymax, M. Houssa, G. Pourtois, F. Bellenger, K. Martens, A. Delabie, S. Van Elshocht, *Appl. Surf. Sci.*, In Press, Corrected Proof, Available online 18 March 2008.
30. J.F. Scott, *Phys. Rev. B*, **1**, 3488 (1970).
31. A. Delabie, M. Caymax, B. Brijs, D. P. Brunco, T. Conard, E. Sleeckx, S. Van Elshocht, L.-Å. Ragnarsson, S. De Gendt, and M. M. Heyns, *J. Electrochem. Soc.*, **153**, F180 (2006).
32. G. D. Wilk, R. M. Wallace, and J. M. Anthony, *J. Appl. Phys.*, **89**, 5243 (2001).
33. R.Castagne, and A.Vapaille, *Surf. Sci.*, **28**, 157 (1971).
34. S. Spiga, C. Wiemer, G. Tallarida, G. Scarel, S. Ferrari, G. Seguini, M. Fanciulli, *Appl. Phys. Lett.*, **87**, 112904 (2005).
35. V. V. Afanas'ev, A. Stesmans, A. Delabie, F. Bellenger, M. Houssa, and M. Meuris, *Appl. Phys. Lett.*, **92**, 022109 (2008).
36. A. Delabie, L. Nyns, F. Bellenger, M. Caymax, T. Conard, A. Franquet, M. Houssa, D. Lin, M. Meuris, L.-Å. Ragnarsson, S. Sioncke, J. Swerts, Y. Fedorenko, J. W. Maes, S. Van Elshocht and S. De Gendt, *ECS Trans.*, **11**, 227 (2007).
37. S. Sioncke, M. Caymax, T. Conard, A. Delabie, A. Franquet, M. Heyns, M. Meuris, A. Urbanczyk, J.L. van Hemmen, W. Keuning, W.M.M. Kessels, *8th international conference on Atomic Layer Deposition (ALD 2008)*, Bruges, Belgium.
38. G. Brammertz, K. Martens, S. Sioncke, A. Delabie, M. Caymax, M. Meuris, M. Heyns, *Appl. Phys. Lett.*, **91**, 133510, 2007.

Downloaded 09 Feb 2009 to 131.155.151.59. Redistribution subject to ECS license or copyright; see http://www.ecsdl.org/terms_use.jsp